ACS OMEGA

Article

Cite This: ACS Omega 2019, 4, 6647−6659

http://pubs.acs.org/journal/acsodf

Effect of Organic Modification on Multiwalled Carbon Nanotube Dispersions in Highly Concentrated Emulsions

Sharu Bhagavathi Kandy,[†,‡,▽] George P. Simon,[§] Wenlong Cheng,[∥] Johann Zank,[#] Kei Saito,[⊥] and Arup R. Bhattacharyya*[,‡]

[†]IITB-Monash Research Academy and [‡]Department of Metallurgical Engineering and Materials Science, Indian Institute of Technology Bombay, Powai, Mumbai 400076, India

[§]Department of Materials Science and Engineering, [∥]Department of Chemical Engineering, and [⊥]School of Chemistry, Monash University, Clayton, Victoria 3800, Australia

[#]Orica Mining Services, George Booth Drive, Kurri Kurri, New South Wales 2327, Australia

[▽]Department of Thermal and Energy Engineering, School of Mechanical Engineering, Vellore Institute of Technology, Vellore, Tamilnadu 632014, India

Supporting Information

ABSTRACT: Highly concentrated water-in-oil emulsions incorporating multiwalled carbon nanotubes (MWCNTs) are prepared. Homogeneous and selective dispersions of MWCNTs throughout the oil phase of the emulsions are investigated. The practical insolubility of carbon nanotubes (CNTs) in aqueous and organic media necessitates the disentanglement of CNT "agglomerates" through the utilization of functionalized CNTs. The design and synthesis of two tetra-alkylated pyrene derivatives, namely, 1,3,6,8-tetra(oct-1-yn-1-yl)pyrene (**TOPy**) and 1,3,6,8-tetra(dodec-1-yn-1-yl)pyrene (**TDPy**), for the noncovalent organic modification of MWCNTs are reported. The modifier molecules are designed in such a manner that they facilitate an improved dispersion of individualized MWCNTs in the continuous-oil phase of the highly concentrated emulsion (HCE). Transmission electron microscopic analyses suggest that the alkylated pyrene molecules are adsorbed on the MWCNT surface, and their adsorption eventually results in the debundling of MWCNT agglomerates. Fourier transform infrared, Raman, and fluorescence spectroscopic analyses confirm the $\pi-\pi$ interaction between the alkylated pyrene molecules and MWCNTs. The noncovalent modification significantly improves the effective debundling and selective dispersion of MWCNTs in HCEs.

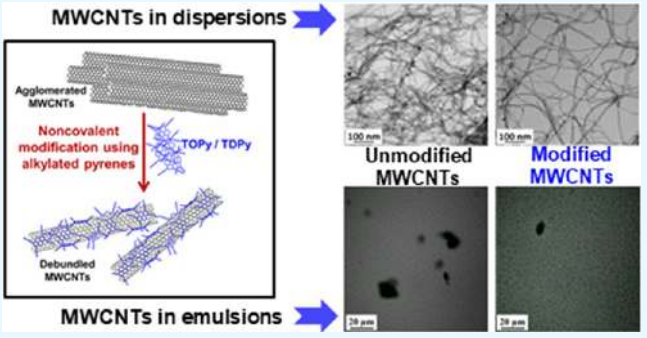

1. INTRODUCTION

Highly concentrated emulsions (HCEs) possess an internal (dispersed) phase volume fraction (ϕ) greater than 0.74, the maximum possible volume fraction of nondeformable monodisperse spheres in hexagonal close packing. In HCEs, ϕ can be as high as 96−99%, and the structure consists of a polydisperse−polyhedral droplet system separated by a thin film of the continuous phase.[1−3] HCEs retain their original structure even at extremely high values of ϕ by virtue of the polydispersity and the deformation of spherical droplets to polyhedral ones.[4,5] Apart from its extensive use in the food industry, cosmetics, paints, oil recovery, and commercial explosives, HCEs are also widely used as reaction media for chemical- and enzyme-catalyzed reactions[6−8] as well as templates for the preparation of low-density materials like poly-high internal phase emulsion (polyHIPE) foams.[9−11] Emulsion explosives that are widely used for commercial blasting in the mining industry are primarily highly concentrated water-in-oil (w/o) emulsions.

Carbon nanotubes (CNTs) are being widely used to improve the thermal, electrical, and mechanical properties of a variety of materials, including ceramics, metals, and polymers. Several studies were reported on HCEs incorporating nanoparticles, including multiwalled carbon nanotubes (MWCNTs), either as Pickering stabilizers or co-stabilizers.[12−16] CNTs with various surface functionalities were incorporated into HCEs to prepare conductive polyHIPE foams with a low electrical percolation threshold.[17−21] A significant level of understanding about the formation of electrically percolating MWCNT networks in HCEs has been gained from these studies on polyHIPE composite foams. Kim et al. have reported a percolation threshold of less than 1 wt % in polyHIPE foams.[18]

Received: November 14, 2018
Accepted: February 20, 2019
Published: April 11, 2019

DOI: 10.1021/acsomega.8b03179
ACS Omega 2019, 4, 6647−6659

In our previous investigation, nanotube-incorporated HCEs were prepared, wherein MWCNTs were added into the continuous phase of w/o HCEs to achieve a MWCNT "network-like" structure within the emulsion.[16] The oil phase of less than 10 wt % of the total emulsion and hence, the MWCNTs network can be achieved with a reasonably low amount of MWCNTs, provided MWCNTs are effectively debundled and selectively dispersed in the oil phase of the emulsion. It is crucial that the MWCNTs should remain in the continuous phase of the emulsion and not diffuse to the oil−water interface, because this may adversely affect the emulsion stability. An efficient MWCNT network within the emulsion could impart additional characteristics or modify the thermal and electrical properties of the emulsion. It is believed that an improvement in the emulsion thermal conductivity could significantly enhance the performance of emulsion explosives.

However, developing a homogeneous dispersion involving "individualized" MWCNTs in the oil blend (which forms the continuous phase of the HCE) remains a difficult task. It was noticed earlier that a fraction of MWCNTs remained in the agglomerated-state in the emulsion matrix.[16] Moreover, the fraction of remaining MWCNT agglomerates increased with the increase in MWCNT concentration in the HCE. CNTs aggregate into bundles or ropes with strong van der Waals interactions during their synthesis, limiting their superior properties.[22] Many of the proposed applications of CNTs have been limited by their poor solubility in aqueous and organic solvents.[23] Hence, it is necessary to debundle the CNT agglomerates to prepare functional CNT-based composites or suspensions.

In view of this, the present investigation focuses on the effective debundling along with the selective dispersion of MWCNTs to localize them in the oil phase of the HCE. Several covalent and noncovalent functionalization strategies were reported to debundle and to disperse CNTs in various dispersion media. Although the covalent functionalization of CNT surfaces can significantly improve the dispersibility of CNTs in various solvents, it alters the sp^2 carbon framework and adversely affects the intrinsic physical properties of CNTs.[23] In contrast, the noncovalent modification of CNTs preserves their intrinsic properties to a great extent, and it involves the adsorption of appropriate modifier molecules onto the CNT surfaces via hydrophobic, van der Waals, and/or electrostatic interactions.[24] Conventional surfactants are not recommended for dispersing MWCNTs in the oil phase of HCEs, as they could disturb the structure and the stability of the emulsion. During the preparation of conductive polyHIPE foams through HCEs, it was noticed that the utilization of water-soluble surfactants to disperse CNTs resulted in unstable HCEs.[18,25] This is because the surfactant destabilizes the film between the droplets, which is stabilized by the emulsifier of the HCE.

Pyrene-containing compounds have often been used for the noncovalent functionalization due to the very high affinity of pyrene toward the CNT surface.[26−37] Pyrene derivatives adsorb on the CNT surface via $\pi-\pi$ interactions, preventing the formation of bundles and enabling its dispersion in solvents.[38,39] Apart from their use as noncovalent stabilizing units, pyrene derivatives were also used to anchor various systems to CNTs in diverse applications. Furthermore, the pyrene ring offers several possibilities of peripheral group modifications, which can affect the condensed-matter structure.[40] It has been reported that the unsubstituted pyrene forms monoclinic crystals, whereas some of the tetra-substituted pyrene derivatives exhibit stacking and form liquid crystalline columnar phases.[41,42]

Noncovalent functionalization of MWCNTs with pyrene derivatives of long hydrocarbon chains may be an efficient way to achieve a stable and selective dispersion of debundled MWCNTs in HCEs. The pyrene ring will ensure the adsorption of the modifier molecules on the surface of the MWCNT through $\pi-\pi$ stacking via coupling of $\pi-\pi$ interactions (between the sp^2 carbons of the aromatic pyrenyl group and MWCNT), and the hydrocarbon chains would interact and allow the MWCNTs to be localized in the oil blend. Two alkylated pyrene derivatives have been chosen for the surface modification of MWCNTs, namely, 1,3,6,8-tetra(oct-1-yn-1-yl)pyrene (**TOPy**) and 1,3,6,8-tetra(dodec-1-yn-1-yl)pyrene (**TDPy**). The two derivatives differ in the side chains that are located on the 1,3,6,8-positions of the pyrene core. **TOPy** consists of an *n*-octyl chain; on the other hand, **TDPy** contains an *n*-dodecyl group. Two alkynes were chosen to assess the influence of the side chain length on the solubilizing power of the modifier molecule. Side chains could have a profound influence on the molecular arrangement as well as on the interaction with the surrounding environment.

These two pyrene derivatives have been synthesized, and their effectiveness as a noncovalent modifier has been investigated in detail. The effect of the noncovalent modification on MWCNT debundling and the interaction between the modifier and MWCNTs were assessed. Furthermore, the modified MWCNTs were incorporated into w/o HCEs, and the influence of noncovalent modification on the dispersion state of MWCNTs was investigated. A model w/o emulsion system with ϕ greater than 90 wt %, which has rheological characteristics identical to those of emulsion explosive precursors, was chosen for this study.

2. RESULTS AND DISCUSSION

2.1. Influence of the Noncovalent Modification on the Morphology and the "Agglomerate State" of MWCNTs. The nature of interactions between MWCNTs and the dispersing medium dictates the "dispersibility" of MWCNTs in a medium. In the case of the modified MWCNTs, the interaction between MWCNTs and the modifier molecules is also important. To establish an understanding of the dispersion state and the extent of the debundling of MWCNTs, the investigation of the dispersion of MWCNTs was carried out at the "microscale" and "nanoscale" levels. The average agglomerate size of MWCNTs was determined by microscale investigations, such as optical microscopy and sedimentation observations, whereas the debundling of MWCNT agglomerates was examined on the nanoscale with the help of scanning electron microscopy (SEM) and transmission electron microscopy (TEM) analyses.

Sedimentation behavior of nanotubes in the presence of the modifier molecule is an important parameter to estimate the dispersibility of MWCNTs. The unmodified and modified MWCNTs were dispersed in tetrahydrofuran (THF), and their sedimentation behavior was examined. The dispersion of the unmodified MWCNTs was highly unstable, and sedimentation was observed after a few minutes of ultrasonication. On the other hand, both 1:1 and 1:2 modified MWCNTs were stable for a few days in THF (Figure S1 in the Supporting Information).

DOI: 10.1021/acsomega.8b03179
ACS Omega 2019, 4, 6647−6659

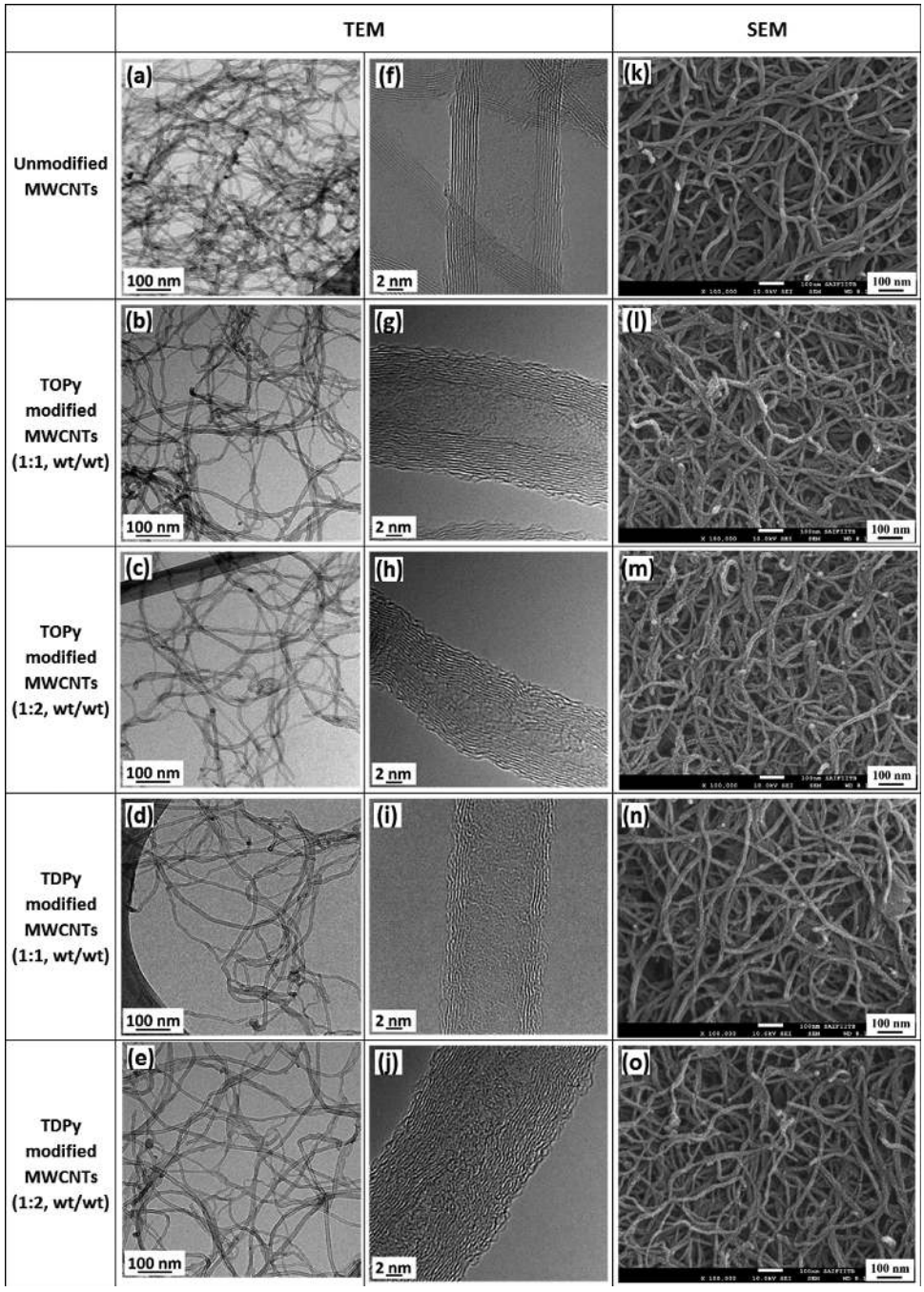

Figure 1. TEM and SEM micrographs of the unmodified and modified MWCNTs: (a)−(e) at 50k magnification; (f−j) high-resolution TEM images of unmodified and modified MWCNTs, at 300k magnification; (k−o) SEM images at 100k magnification.

Furthermore, dispersion studies of MWCNTs were carried out in the oil blend, where the oil blend composition was the same as that of the continuous phase of the emulsion (Figure S2 in the Supporting Information). This investigation could provide crucial insights into the influence of the noncovalent modification on the dispersion state of MWCNTs in the oil phase of the emulsion. The size of the MWCNT agglomerates that remained in the oil blend−MWCNT dispersion was determined using optical microscopic analysis for the unmodified and modified MWCNTs (Figure S2 in the Supporting Information). The average agglomerate size for the unmodified MWCNTs was observed to be ∼218.2 μm^2, whereas for 1:1 (w/w) **TOPy**- and **TDPy**-modified MWCNTs, it was ∼109.9 and ∼93.4 μm^2, respectively (Figure S3 in the Supporting Information). With the increase in the modifier weight ratio, the agglomerate size was further reduced to ∼75.6 and ∼73.2 μm^2, respectively, for the 1:2 (w/w) **TOPy**- and **TDPy**-modified MWCNTs. Thus, the dispersion with unmodified MWCNTs exhibited a higher average agglomerate size as compared to all corresponding modified MWCNTs. However, there was no significant variation in the average agglomerate sizes of modified MWCNTs, between these two modifiers at a specific modifier concentration. For the modified MWCNTs, the average size of MWCNT agglomerates reduced with increasing weight ratio of **TOPy** and **TDPy**. Similar observations were reported for MWCNTs

DOI: 10.1021/acsomega.8b03179
ACS Omega 2019, 4, 6647−6659

that were surface-modified using 1-pyrenecarboxaldehyde and sodium/lithium salt of 6-aminohexanoic acid.[43,44]

Pyrene derivatives have been reported to interact with the nanotube surface with a high surface coverage because of the very high affinity of pyrene toward the CNT surface.[26,27,30−34] Pyrene derivatives adsorb onto the surface of CNTs through $\pi-\pi$ interactions, preventing the bundle formation and enabling its dispersion in solvents.[38,39] It is also likely that the **TOPy** and **TDPy** molecules may form a "layer-like structure", while covering the surface of MWCNTs, owing to better packing offered by the matching aromatic structure. Lerner et al. demonstrated the stacking of pyrene molecules on a nanotube surface through an increased thickness of the nanotube, as observed in AFM studies.[38] Furthermore, it was demonstrated through molecular simulation that the stability of the complex of pyrene with the nanotube is greater than that between two pyrene molecules.[27] Thus, the pyrene molecule and its derivatives have the tendency to interact with the nanotube surface and form a complex rather than assembling themselves.

The morphology of the unmodified and modified MWCNTs, as observed in TEM and SEM analyses, is shown in Figure 1. The unmodified MWCNTs exhibited a highly agglomerated state, whereas the **TOPy**- and **TDPy**-modified MWCNTs showed a less agglomerated state. TEM micrographs (Figure 1a−e) illustrate the debundling of MWCNTs upon modification. As observed from the high-resolution TEM (HR-TEM) micrographs, which were imaged at 300k magnification, the unmodified MWCNTs show a relatively smooth surface (Figure 1f), whereas the TEM micrographs of the modified MWCNTs exhibit roughness on the outer wall, which is expected to have originated from the modifier molecules that adhered to the surface of the MWCNTs (Figure 1g−j). The SEM micrographs of unmodified and modified MWCNTs depict an "entangled" network of MWCNTs. However, it is expected that the "agglomerate-strength" of the MWCNTs may decrease with the modification due to the effective debundling.

Furthermore, the average diameters of the unmodified and modified MWCNTs were estimated from the HR-TEM images. The increase in the average diameter of MWCNTs suggests the adsorption of the modifier molecules on the MWCNT surface. Average diameters of the unmodified and modified MWCNTs that were estimated from the TEM micrographs are shown in Table 1. SEM and TEM

Table 1. Average Diameter (Determined from HR-TEM Images) of the Unmodified and Modified MWCNTs

sample		D_{avg} (nm)
unmodified MWCNTs		10.2 ± 2
TOPy-modified MWCNTs	1:1 (w/w)	12.4 ± 1
	1:2 (w/w)	12.3 ± 1.7
TDPy-modified MWCNTs	1:1 (w/w)	13.2 ± 2.5
	1:2 (w/w)	14.3 ± 1.4

observations suggest that the **TOPy** and **TDPy** molecules are adsorbed on the MWCNT surface to a thickness of ca. 1.5−2 nm, and this subsequently results in debundling of the MWCNT agglomerates. The **TOPy** and **TDPy** molecules interact with the MWCNT surface through $\pi-\pi$ interactions and these adsorbed molecules weaken the intertube attractive forces resulting in the debundling of MWCNTs.

2.2. Interaction between Alkylated Pyrene Modifier Molecules and MWCNTs. The performance of CNT-based nanocomposites and suspensions relies strongly on the interaction of CNTs with their environment, which is in turn influenced by the chemical structure and nature of the dispersion medium and the presence of other modifier molecules. There can be various noncovalent interactions that act between CNTs and molecular, macromolecular, or ionic species that constitute the dispersion medium.[33] The highly aromatic nature of the pyrenyl group leads to a strong $\pi-\pi$ interaction with the sidewalls of CNTs.[45] Various techniques, such as fluorescence spectroscopy, Fourier transform infrared (FTIR), Raman spectroscopy, and NMR can be used to probe the $\pi-\pi$ interaction between the pyrene derivative molecules and CNTs.[27] A detailed assessment of interactions between the modifier molecules and MWCNTs would bring interesting insights into the understanding of MWCNT dispersions in the oil phase of emulsions that have been investigated here. FTIR spectra, Raman spectra, and fluorescence emission spectra of unmodified and modified MWCNTs were analyzed to assess the interaction between the modifier molecules and MWCNTs.

2.2.1. FTIR Spectroscopic Measurements. FTIR spectra of unmodified, 1:1 **TOPy**-, and 1:1 **TDPy**-modified MWCNTs in the full wavelength range is presented in Figure S4 in the Supporting Information. Figure 2a exhibits the FTIR spectra of

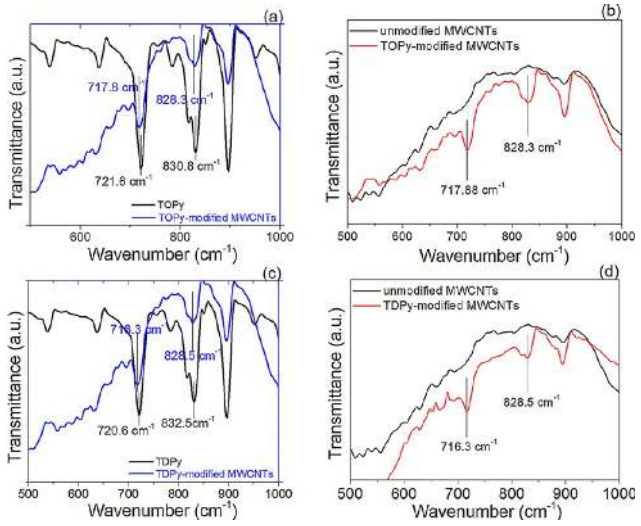

Figure 2. FTIR spectra of (a) **TOPy** and 1:1 (w/w) **TOPy**-modified MWCNTs; (b) unmodified and 1:1 (w/w) **TOPy**-modified MWCNTs; (c) **TDPy** and 1:1 (w/w) **TDPy**-modified MWCNTs; (d) unmodified and 1:1 (w/w) **TDPy**-modified MWCNTs.

TOPy and 1:1 **TOPy**-modified MWCNTs. As observed from the FTIR spectrum of **TOPy**, the peaks at 721.6 and 830.8 cm^{-1} are associated with the C−H wagging vibrations of the pyrenyl group. These two wagging vibration bands appeared in the **TOPy**-modified MWCNTs as well. However, they showed a downshift to 717.8 and 828.3 cm^{-1}. These downshifts of the wagging vibrational peaks indicate the strong $\pi-\pi$ stacking interaction and the possible hydrophobic interactions between the aromatic rings of **TOPy** and the MWCNT surface.[27,43] Figure 2b shows the FTIR spectra of the unmodified and 1:1 **TOPy**-modified MWCNTs. Figure 2c illustrates the downshift of the wagging vibrational bands in **TDPy**-modified MWCNTs. The vibrational bands have shown a downshift to

DOI: 10.1021/acsomega.8b03179
ACS Omega 2019, 4, 6647−6659

716.3 and 828.5 cm^{-1}, respectively, from 720.6 and 832.5 cm^{-1} corresponding to **TDPy**. Figure 2d shows the FTIR spectra of the unmodified and 1:1 **TDPy**-modified MWCNTs. Thus, a shift of the wagging vibrational bands to lower wavenumbers suggests the strong $\pi-\pi$ interaction between the aromatic rings of the modifier molecules and the MWCNT surface.

2.2.2. Raman Spectroscopic Measurements. Figure 3a shows the Raman spectra of unmodified, **TOPy**-, and **TDPy**-

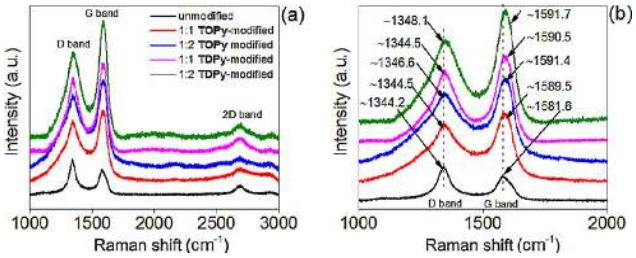

Figure 3. Raman spectroscopic investigation of the unmodified and modified MWCNTs: (a) Raman spectra in the full scan range for unmodified, **TOPy**-, and **TDPy**-modified MWCNTs; (b) Raman spectra in the 1000−2000 cm^{-1} range, illustrating the shifts in the D-band and G-band of the modified MWCNTs.

modified MWCNTs. The Raman spectrum of the unmodified MWCNTs exhibits two characteristic peaks: a D-band at ∼1344.2 cm^{-1} and a G-band centered at ∼1581.6 cm^{-1}. Raman scattering involves inelastic scattering of light, and the Raman spectrum depicts the scattered light intensity with respect to the excitation wavelength. The shape and intensity of the D-band correspond to the sp^3 hybridized carbon atoms,[46] which is correlated with the defect concentration or the measure of disorders in the C−C bonds and the chemical sidewall functionalization.[47] The G-band is attributed to the tangential C═C bond stretching in an ordered graphitic structure.[48]

Raman spectra of unmodified and modified MWCNTs in the range of 1000−2000 cm^{-1} are shown in Figure 3b to clearly illustrate the shifts in the characteristic peaks of the modified MWCNTs. The Raman spectra of the modified MWCNTs exhibit an upward shift in the G-band: ∼1589.5 and ∼1591.4 cm^{-1} for 1:1 and 1:2 (w/w) **TOPy**-modified MWCNTs, respectively; ∼1590.5 and ∼1591.7 cm^{-1} for 1:1 and 1:2 (w/w) **TDPy**-modified MWCNTs, respectively. Furthermore, the D-band of the modified MWCNTs also exhibited an upward shift, but relatively lower when compared to that of the G-band: ∼1346.5 and ∼1348.5 for 1:2 (w/w) **TOPy**- and **TDPy**-modified MWCNTs, respectively.

The D-band and G-band peaks originate due to the "resonance phenomenon", and the peak position could be associated with the electronic and vibrational densities of state.[43] The adsorption of the alkylated pyrene molecules on MWCNTs may alter the vibrational densities of state and could eventually affect the vibrational modes of MWCNTs. Furthermore, the tangential displacement G-mode is also sensitive to the charge that is exchanged between the CNTs and the adsorbed molecule.[49] Hence, the shift in the G-band to a higher wavenumber for the modified MWCNTs could be due to the $\pi-\pi$ interaction between the adsorbed modifier molecules and MWCNTs. A similar shift to higher wavelengths in the Raman spectroscopic peaks of pyrene-modified MWCNTs has been reported earlier.[27] Furthermore, a shift to a higher wavenumber can also arise due to weaker intertube interactions, suggesting the "de-agglomeration" of MWCNTs in the presence of the modifier molecules.

The unmodified MWCNTs exhibit a I_D/I_G value of ∼1.22, whereas the 1:1 and 1:2 (w/w) **TOPy**-modified MWCNTs show ∼0.82 and ∼0.98, respectively. For the **TDPy**-modified MWCNTs, the I_D/I_G values are 0.95 and 0.99, respectively, for 1:1 and 1:2 (w/w) modifications. An increase in the I_D/I_G ratio indicates a higher defect fraction in the ordered graphitic structure.[43,50] Furthermore, a reduced I_D/I_G ratio suggests an improved debundling of MWCNT agglomerates and an enhanced resonance process after the exfoliation of MWCNTs.[51,52] The persistent decrease in the I_D/I_G ratio of modified MWCNTs is due to the enhanced debundling of MWCNTs in the presence of alkylated pyrene molecules.

2.2.3. UV−Visible and Fluorescence Spectroscopy Measurements. The UV−visible absorption spectra of unmodified, 1:2 (w/w) **TOPy**-, and **TDPy**-modified MWCNT dispersions in THF along with the absorption spectra of **TOPy** and **TDPy** free molecules in THF are shown in Figure 4. The unmodified

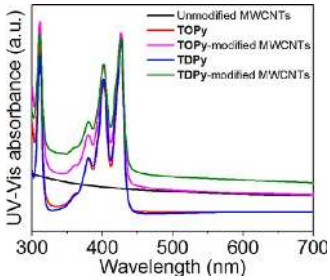

Figure 4. UV−visible absorption spectra of dilute solutions of **TOPy** and **TDPy**, and dispersions of unmodified, **TOPy**-, and **TDPy**-modified MWCNTs in THF.

MWCNTs in THF exhibited an absorption maximum at ∼253 nm. The absorption spectra of both modified MWCNTs were almost identical to those of the free modifier molecules in THF. This observation implies that the absorption spectrum is primarily governed by the respective modifier molecules in the corresponding bulk solution.

Fluorescence spectra of the pyrene monomers in the solution phase show significant vibronic bands, and the pyrene derivatives are often used as fluorescence probes due to their high fluorescence quantum yield.[27,53] The strong fluorescence from the **TOPy** and **TDPy** molecules is a marker to demonstrate the interaction of these molecules with MWCNTs. The fluorescence spectra of **TOPy**- and **TDPy**-modified MWCNT dispersions in THF were recorded using solutions that possessed identical absorbance at the Soret band maximum (426 nm). Figure 5 exhibits the fluorescence emission spectra of all materials in THF. Upon excitation, the fluorescence spectra of the modified MWCNTs show superimposable profiles with respect to the free **TOPy** and **TDPy** molecules in THF. Although there is no change in the spectroscopic feature for both modified MWCNTs, a significant quenching in the fluorescence emission intensity of the modified MWCNTs is observed when compared to the emission intensity of the modifier molecules alone in THF. However, there is no significant spectral shifting in the presence of MWCNTs. Fluorescence quenching by CNTs through energy transfer has been reported in several publications.[27,32,54−59] The fluorescence quenching is attributed to the energy transfer from the high-energy pyrene singlet

DOI: 10.1021/acsomega.8b03179
ACS Omega 2019, 4, 6647−6659

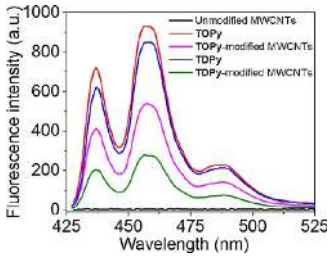

Figure 5. Fluorescence emission spectra of dilute solutions of **TOPy** and **TDPy**, and dispersions of unmodified, **TOPy**-, and **TDPy**-modified MWCNTs in THF. All samples, except for the dispersions of unmodified MWCNTs, possessed a matching absorption at 426 nm. This is a qualitative trend of the fluorescence emission intensities and cannot be assumed to be quantitative for comparisons (λ_{ex} = 426 nm, excitation and emission slit width is 2.5 nm).

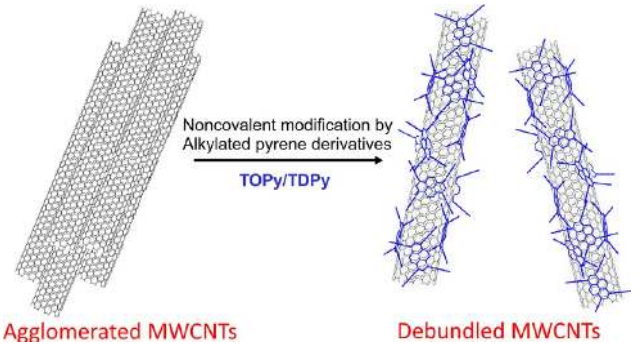

Figure 6. Schematic representation of physical adsorption of alkylated pyrene derivatives on the surface of MWCNTs leading to the debundling of MWCNT agglomerates (the dimensions of MWCNTs and modifier molecules are not in scale).

which is at the excited state to the low-energy manifold of CNTs.[60] The residual fluorescence might be derived from the free, nonimmobilized modifier molecules in the solution.

To further investigate the interaction between the modifier molecules and MWCNTs at the molecular level, a set of fluorescence spectroscopy experiments were run at varied concentrations of MWCNTs in the modifier solution in THF. Upon excitation, the fluorescence spectra of MWCNTs again showed superimposable profiles with respect to the free **TOPy** and **TDPy** molecules in THF. The addition of MWCNTs did not give rise to a new spectroscopic feature; however, there was substantial quenching in the fluorescence emission intensity in the presence of MWCNTs when compared to the emission intensity of the modifier molecules alone in THF (Figure S5 in the Supporting Information).

The fluorescence measurements strongly suggest a mapping of the modifier molecules onto the surface of the MWCNTs through $\pi-\pi$ stacking. Thus, the residual fluorescence quenching may presumably be due to $\pi-\pi$ interactions. Since there is no indication of charge transfer between the modifier molecule and MWCNTs, the fluorescence quenching could have resulted from an efficient energy transfer from the pyrene moiety in **TOPy** and **TDPy** to the MWCNTs through vibrational coupling. However, it is also reported that the observed reduction in the fluorescence intensity cannot be assumed to be quantitative. Fluorescence quenching could also result from other factors such as light partitioning between the modifier molecule and the MWCNTs (hence, a fraction of the photons excites the CNT scaffold) and scattering of the emitted light due to the presence of MWCNTs in the dispersion.[58,61]

Figure 6 illustrates the schematic of the noncovalent modification of MWCNTs using the alkylated pyrene derivatives, which leads to the debundling of MWCNT agglomerates. Details of the interaction between the alkylated pyrene modifier molecules and MWCNTs at the molecular level are indefinite at the current stage. However, the spectroscopic results suggest that the physical adsorption of the modifier molecules on the sidewall of the MWCNTs can be attributed to $\pi-\pi$ interactions and van der Waals interactions.

2.3. Modified MWCNT-Incorporated HCEs. To facilitate the selective dispersion and localization, MWCNTs were originally dispersed in the oil blend through ultrasonication. The oil blend comprises a mixture of hydrocarbon oils and an emulsifier. The oil blend−MWCNT dispersion was used as the oil phase for the preparation of the nanotube-incorporated HCE and gradually incorporated into the salt solution to prepare the emulsion. First, a stable and homogeneous dispersion of the individualized MWCNTs in the oil blend is necessary to effectively incorporate MWCNTs into the emulsion matrix. Even though the modified MWCNTs could provide a much improved dispersion of debundled MWCNTs in the oil blend, some amount of MWCNTs still remained in the agglomerated state. This could be due to the very high concentration of MWCNTs in the oil blend. The amount of modified MWCNTs in the dispersion ranged between 2.24 and 17.9 mg/mL and was considerably higher when compared to the other high-concentration CNT dispersions reported in any organic solvent (~2 mg/mL).[62] Even an extended ultrasonication also failed to cause any considerable improvement in the dispersion state of MWCNTs. The remaining MWCNT agglomerates were more noticeable in dispersions that had a higher loading of MWCNTs. The MWCNT−oil blend dispersions of unmodified and modified MWCNTs with varying concentrations of MWCNTs were used for preparing the nanotube-incorporated HCEs.

2.3.1. Emulsion Microstructure. Laser scanning confocal microscopy was used to obtain differential interference contrast (DIC) images and fluorescence images of emulsions. Figure 7 illustrates the fluorescence images and overlapped DIC-fluorescence images for 0.5NT and 1NT emulsions incorporated with modified MWCNTs when excited with a laser at 488 nm. Emulsions incorporated with modified MWCNTs exhibit fluorescence, which arises from the adsorbed alkylated pyrene molecules excited by the laser (Figure 7a−h). As observed from micrographs, the fluorescence phenomenon is from the thin layer around the dispersed droplets, which suggests that a major fraction of the MWCNTs is localized and confined to the continuous phase of HCEs (Figure 7a−h). It should also be noted that there is a possibility that some fraction of the adsorbed modifier molecules from the modified MWCNTs gets dissolved in the oil blend. This might also contribute to the total fluorescence from the continuous phase.

The modified MWCNTs allow better dispersion of the individualized MWCNTs, as well as allow them to be localized in the continuous phase of the emulsion so that the MWCNT network can be achieved within the HCE. Laser scanning confocal microscopic analyses qualitatively suggest that the majority of MWCNTs remain selectively dispersed in the continuous phase of the emulsion; however, some fraction of

DOI: 10.1021/acsomega.8b03179
ACS Omega 2019, 4, 6647−6659

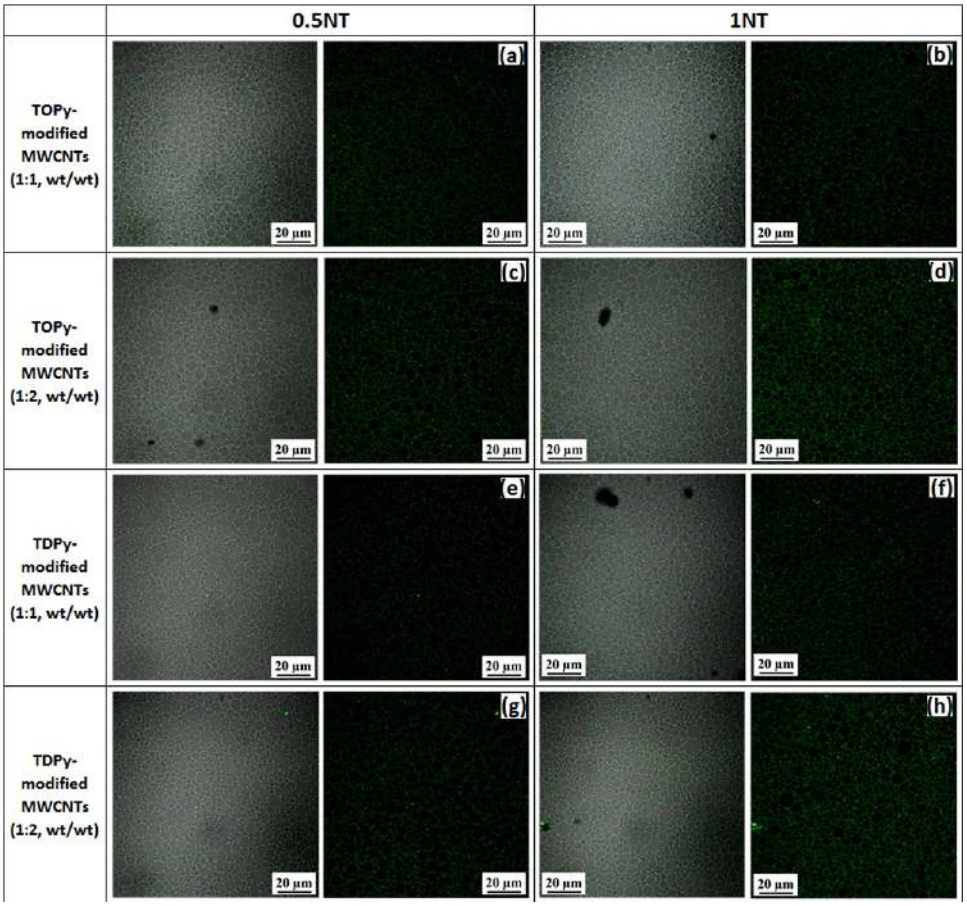

Figure 7. Laser scanning confocal micrographs of emulsions incorporated with modified MWCNTs, which show fluorescence images (right) and overlapped DIC-fluorescence images (left) for 0.5NT and 1NT emulsions: (a–d) emulsions incorporated with 1:1 and 1:2 (w/w) **TOPy**-modified MWCNTs; (e–h) emulsions incorporated with 1:1 and 1:2 (w/w) **TDPy**-modified MWCNTs.

MWCNTs remained in the agglomerated state in the emulsion matrix. Furthermore, it needs to be investigated whether the amount of MWCNTs dispersed in the HCE is sufficient to alter any emulsion characteristics by forming an efficient three-dimensional network within the HCE. On the other hand, it is not possible to incorporate a very high amount of MWCNTs into the oil phase as any concentration beyond ∼5 wt % in the oil phase hardly produces stable emulsions or cannot accommodate the same, very high, aqueous phase volume fraction, even when some emulsions are formed.

2.3.2. Dispersion State of the MWCNTs in the Emulsion: Microscale and Nanoscale Analyses. 2.3.2.1. Average Agglomerate Size of the MWCNTs in the Emulsion: Influence of Noncovalent Modification. Microscopic analyses were carried out to assess the role of the noncovalent modifiers in effectively debundling the agglomerates of MWCNTs to achieve an improved dispersion in the emulsion. The size of the MWCNT agglomerates that remained in the emulsion matrix was determined using confocal microscopic analysis (Figure 8a–l). It can be seen that the remaining MWCNT agglomerates are more prominent in emulsions with unmodified MWCNTs (Figure 8a–d), whereas a substantial improvement is observed in the case of emulsions with modified MWCNTs (Figure 8e–l).

Around 25–30 micrographs were analyzed for each emulsion system, and the data numerically processed to assess the enhancement of MWCNT dispersion in the corresponding emulsion. Figure 9 demonstrates the variation in average agglomerate size (D_{avg}) and the percentage area of agglomerates in the unmodified and 1:2 (w/w) modified nanotube-incorporated emulsions with different concentrations of MWCNTs. For the emulsion having 0.25 wt % MWCNTs, D_{avg} is 9.8 μm for the unmodified MWCNTs, whereas for the **TOPy**- and **TDPy**-modified MWCNTs, it is 6.8 and 6.5 μm, respectively. For the 2 wt % nanotube-incorporated emulsions, D_{avg} is 12.4 μm for the unmodified MWCNTs and 10.6 and 10.9 μm, respectively, for the **TOPy**- and **TDPy**-modified MWCNTs. Furthermore, the trend in the calculated area ratios of the agglomerates is consistent with that of the agglomerate size. For 0.25NT and 2NT emulsions incorporated with unmodified MWCNTs, the area ratio is 0.55 and 8.8%, respectively. In contrast, the corresponding area ratios are 0.18 and 5.5% for the emulsions incorporated with **TOPy**-modified MWCNTs and 0.21 and 5.1% for the emulsions incorporated with **TDPy**-modified MWCNTs.

The microscale analysis suggests that the noncovalent surface modification has effectively improved the dispersion state of the MWCNTs in the emulsion. This can be envisaged as a result of the effective debundling of the MWCNTs in the presence of the noncovalent modifier molecules. Moreover, the rapid re-aggregation of the dispersed MWCNTs might have been hindered by the adsorbed modifier molecules on the MWCNT surface. It is also expected that the noncovalent modification facilitates the localization of the individualized MWCNTs predominantly in the oil phase mediated via the specific interaction between the alkyl chain of the organic

DOI: 10.1021/acsomega.8b03179
ACS Omega 2019, 4, 6647–6659

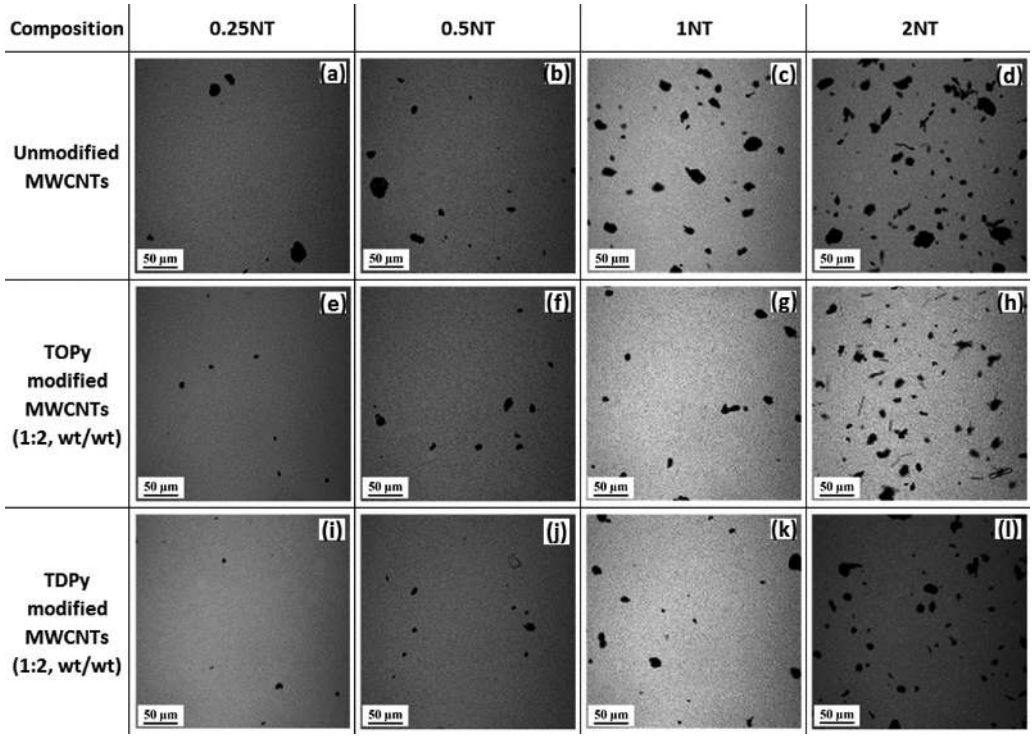

Figure 8. Laser scanning confocal micrographs that show the remaining MWCNT agglomerates in the 0.25NT, 0.5NT, 1NT, and 2NT emulsions incorporated with unmodified and modified MWCNTs: (a–d) emulsions incorporated with unmodified MWCNTs; (e–h) emulsions incorporated with 1:2 (w/w) **TOPy**-modified MWCNTs; and (i–l) emulsions incorporated with 1:2 (w/w) **TDPy**-modified MWCNTs.

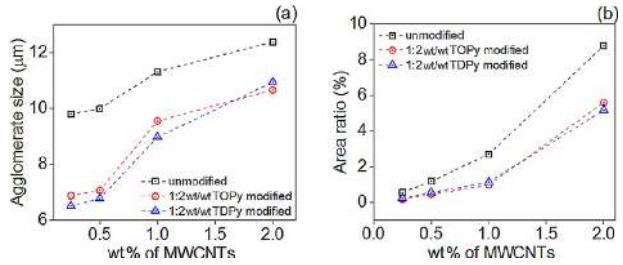

Figure 9. Variation in the (a) average agglomerate size and (b) area ratio of the MWCNT agglomerates that remained in the emulsion matrix for the emulsions incorporated with unmodified and modified MWCNTs.

modifier and the oil phase. At room temperature, the dispersed aqueous droplets are made of a supersaturated and supercooled salt solution. Hence, it is crucial that the dispersed MWCNTs stay in the continuous-oil phase of the emulsion and not migrate to the oil–water interface, as this may adversely affect the stability of the emulsion.

2.3.2.2. Dispersion State of MWCNTs in HCEs: Nanoscale Microstructural Analysis Using Cryo-FEG-SEM. Cryo-FEG-SEM analysis was performed to assess the dispersion state of MWCNTs at the nanoscale level. The dispersion state of various MWCNTs has been analyzed by considering the 1NT emulsion samples as the representative emulsions. The emulsion samples were frozen at −190 °C, and the corresponding SEM images were taken from the fractured surfaces. The morphologies of the 1NT emulsion incorporated with unmodified MWCNTs (Figure 10a,b), the corresponding emulsion incorporated with 1:2 (w/w) **TOPy**-modified MWCNTs (Figure 10c,d), and the corresponding emulsion incorporated with 1:2 (w/w) **TDPy**-modified MWCNTs (Figure 10e,f) are shown in the SEM micrographs (Figure 10a–f). The morphology, as observed from the Cryo-FEG-SEM micrographs, suggests that it is quite difficult to differentiate between the dispersion states of different MWCNTs in the corresponding emulsions. The dispersed MWCNTs in the emulsion matrix can be clearly observed in the micrographs of fractured surfaces. However, the selective dispersion and localization of MWCNTs in the oil phase of HCEs cannot be explicitly established from these micrographs. Hence, the Cryo-FEG-SEM observation of the fractured surface morphology alone is inadequate to elucidate the dispersion states of the unmodified and modified MWCNTs in the respective emulsions.

3. CONCLUSIONS

Two tetra-alkylated pyrene derivatives that can act as effective noncovalent surface modifiers for MWCNTs were proposed and synthesized. The tetra-alkylated pyrene molecules were intended to produce a better dispersion of the individualized MWCNTs, and allow them to be localized in the continuous-oil phase of the highly concentrated w/o emulsions. These modifier molecules interact efficiently with the MWCNT surface through $\pi-\pi$ interactions. The adsorption of the modifier molecules onto the surface of the MWCNTs resulted in the effective debundling of MWCNT agglomerates due to the weakened force of attraction between the nanotubes. Both the G-band shift in Raman spectroscopic analysis and the downshift of wagging vibrational bands in FTIR analysis, which were exhibited by the modified MWCNTs, along with the fluorescence quenching of the alkylated pyrene molecules in the presence of the MWCNTs all confirm the $\pi-\pi$ interaction between the tetra-alkylated pyrene molecules and MWCNTs.

DOI: 10.1021/acsomega.8b03179
ACS Omega 2019, 4, 6647–6659

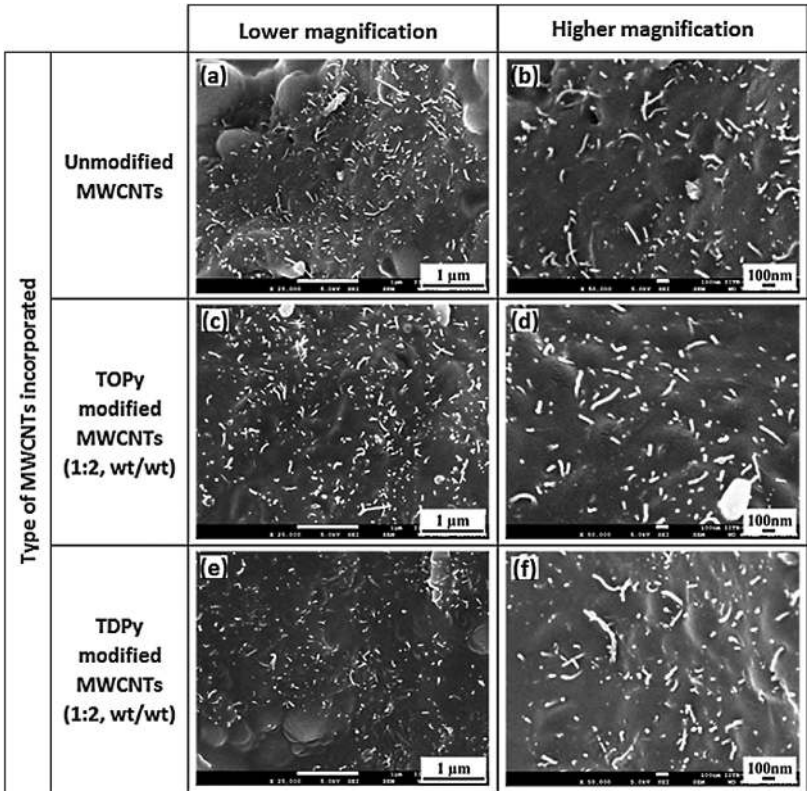

Figure 10. Cryo-FEG-SEM images of 1NT emulsion incorporated with unmodified and modified MWCNTs at high and low magnifications: (a, b) 1NT emulsion incorporated with unmodified MWCNTs; (c, d) 1NT emulsion incorporated with 1:2 (w/w) **TOPy**-modified MWCNTs; (e, f) 1NT emulsion incorporated with 1:2 (w/w) **TDPy**-modified MWCNTs.

The modified MWCNTs were then incorporated into HCEs, and the influence of the noncovalent surface modification on the MWCNT dispersion in emulsions was investigated. The fluorescence localization from the thin layer around the dispersed droplets, in emulsions incorporated with modified MWCNTs, suggested that the major fraction of the incorporated MWCNTs are localized and confined to the continuous-oil phase of HCEs. However, the selective dispersion and localization of MWCNTs in the oil phase of HCEs was not unambiguously concluded from the Cryo-FEG-SEM micrographs. Developing an efficient protocol to investigate the state of dispersion of MWCNTs in these emulsions is important and extremely challenging. Moreover, a comparatively minor fraction of MWCNTs remained in the agglomerated state in the emulsion, even after the noncovalent modification. However, there was a substantial reduction in the average size and the area ratio of the MWCNT agglomerates that remained in the emulsion matrix in these emulsions when compared to the corresponding emulsions composed of unmodified MWCNTs. However, there was no significant difference in the average agglomerate sizes of modified MWCNTs between the two modifiers. The improved dispersion state of MWCNTs in the emulsion can be envisaged as a result of the effective debundling in the presence of the noncovalent modifier molecules and the impeded rapid re-aggregation of the dispersed MWCNTs by the adsorbed modifier molecules.

4. EXPERIMENTAL SECTION

4.1. Materials. *4.1.1. Synthesis of Alkylated Pyrenes.* 1,3,6,8-Tetrabromopyrene, 1-octyne, 1-dodecyne, bis-(triphenylphosphine)palladium(II) dichloride ($Pd(PPh_3)_2Cl_2$) and copper(I) iodide (CuI) were procured from Sigma-Aldrich. The solvents, dichloromethane (DCM) and petroleum benzine, were procured from Merck Ltd., and anhydrous tetrahydrofuran (THF) and diisopropylamine were obtained from Sigma-Aldrich.

4.1.2. Emulsion Preparation. All of the constituents of the oil phase of the emulsion, such as the methylated canola oil, Exxol D130 (paraffinic oil), and emulsifier (polyisobutylene succinic anhydride (PIBSA)−diethanolamine derivative surfactant) were supplied by Orica Australia Pty. Ltd. The emulsifier is based on alkanolamine derivatives of PIBSA, which is prepared by reacting PIBSA and diethanolamine in 1:1 M ratio. Further details of the PIBSA-derivative emulsifier can be found elsewhere.[16] The constituents of the aqueous phase, such as ammonium sulfate, ammonium chloride, and other trace additives, were procured from Sigma-Aldrich. Deionized water was used to prepare the aqueous phase, and the trace additives were added to adjust the pH of the salt solution. MWCNTs were procured from Nanocyl S.A., Belgium (grade: NC 3100; D_{avg} = 9.5 nm, L = 1.5 μm and purity greater than 95% as per manufacturer).

4.2. Synthesis. *4.2.1. General Methods.* Thin-layer chromatography was performed using silica gel plates (Merck) that were precoated with a fluorescent indicator with visualization by ultraviolet light. Column chromatography was performed on silica gel (60−120 mesh). ^{1}H and ^{13}C NMR spectra were recorded using a Bruker Avance-400 spectrometer (^{1}H: 400 MHz and ^{13}C: 100 MHz). The chemical shifts are recorded in ppm using the solvent as an internal standard: chloroform-*d* at 7.24 and 77.23 ppm for ^{1}H and ^{13}C NMR,

DOI: 10.1021/acsomega.8b03179
ACS Omega 2019, 4, 6647−6659

respectively. High-resolution mass spectra (HRMS) were recorded using a Q-TOF analyzer in the positive ion electrospray ionization (ESI) mode.

TOPy has previously been synthesized.[40,63] The synthesis protocol of **TDPy** was adapted from that of **TOPy**. Tetrabromopyrene was functionalized with 1-octyne and 1-dodecyne under Sonogashira conditions to obtain **TOPy** and **TDPy**, respectively. Synthesis protocols for **TOPy** and **TDPy** are detailed below:

1,3,6,8-Tetrabromopyrene (2 g, 3.86 mmol), CuI (42 mg, 0.22 mmol), and $(Pd(PPh_3)_2Cl_2)$ (142 mg, 0.202 mmol) were added to a degassed solution of anhydrous THF (40 mL) and diisopropylamine (40 mL) in a round-bottomed flask under N_2. The mixture was again degassed and an excess of 1-octyne (4 mL, 27.11 mmol, 7 equiv) was added. The mixture was degassed once again and stirred at 80 °C under N_2 for 24 h. The reaction mixture was then allowed to cool to room temperature and, subsequently, filtered over celite and washed with 250 mL of DCM. The solvent was then removed, and the residue was dried under vacuum. The crude product was purified by column chromatography with a solvent that comprised 90% of petroleum benzine and 10% of DCM. Furthermore, precipitation from DCM−diethyl ether yielded a bright yellow powder of **TOPy** (1.36 g, 55.6% yield) (Scheme 1).

Scheme 1. 1,3,6,8-Tetra(oct-1-yn-1-yl)pyrene (TOPy)

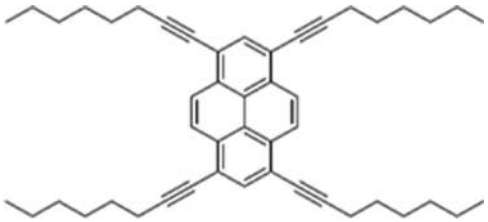

Melting point: 95.6 °C. ^{1}H NMR (400 MHz, $CDCl_3$): δ 8.57 (s, 4H); 8.17 (s, 2H); 2.66 (t, 8H); 1.79 (m, 8H); 1.61 (m, 8H); 1.43 (m, 16H); 0.97 (m, 12H) ppm (Figure S6 in the Supporting Information). ^{13}C NMR (100 MHz, $CDCl_3$): δ 133.6, 131.4, 126.3, 124.1, 119.3, 97.0, 79.0, 31.4, 28.9, 28.8, 22.7, 19.9, 14.1 ppm (Figure S7 in the Supporting Information). HRMS (ESI): calcd for $C_{48}H_{58}Na$ $[(M + Na)]^+$ 657.4431; found, 657.4435 (Δm +0004 and error +0.6 ppm).

1,3,6,8-Tetrabromopyrene (2 g, 3.86 mmol), CuI (58 mg, 0.30 mmol), and $Pd(PPh_3)_2Cl_2$ (164 mg, 0.23 mmol) were added to a degassed solution of anhydrous THF (40 mL) and diisopropylamine (40 mL) in a round-bottomed flask under N_2. The mixture was again degassed and an excess of 1-dodecyne (3 mL, 14.03 mmol, 7 equiv) was added. The mixture was degassed once again and stirred at 85 °C under N_2 for 24 h. The resulting mixture was filtered over celite and washed with 250 mL of DCM. The solvent was then removed, and the residue was dried under vacuum. The crude product was purified by column chromatography with a solvent that comprised 90% of petroleum benzine and 10% of DCM. Precipitation from DCM−diethyl ether yielded a bright yellow powder of **TDPy** (684 mg, 40% yield) (Scheme 2).

Melting point: 81.8 °C. ^{1}H NMR (400 MHz, $CDCl_3$): δ 8.57 (s, 4H); 8.17 (s, 2H); 2.65 (t, 8H); 1.78 (m, 8H); 1.6 (m, 8H); 1.3 (m, 48H); 0.90 (m, 12H) ppm (Figure S8 in the Supporting Information). ^{13}C NMR (100 MHz, $CDCl_3$): δ 133.62, 131.38, 126.35, 124.08, 119.28, 96.96, 78.99, 31.92, 29.62, 29.58, 29.35, 29.2, 29.08, 28.94, 22.69, 19.92, 14.1 ppm (Figure S9 in the Supporting Information). HRMS (ESI): calcd for $C_{64}H_{90}Na$ $[(M + Na)]^+$ 881.6935; found, 881.6931 (Δm +0004 and error +0.4 ppm). FTIR, UV−visible, and fluorescence spectra of **TOPy** and **TDPy** are provided in Figures S10 and S11 in the Supporting Information.

Scheme 2. 1,3,6,8-Tetra(dodec-1-yn-1-yl)pyrene (TDPy)

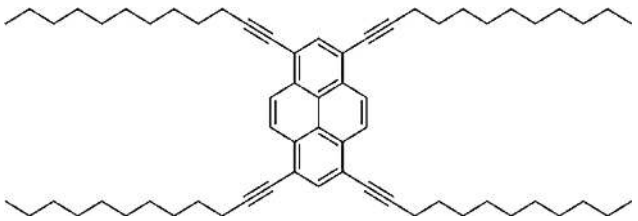

4.3. Surface Modification of MWCNTs Using Alkylated Pyrene Molecules. Both **TOPy** and **TDPy** demonstrated very high solubility in common organic solvents, such as hexane, toluene, chloroform, DCM, and THF. MWCNTs were solubilized in THF, and subsequently, the **TOPy**- and **TDPy**-functionalized MWCNTs were prepared. MWCNT/modifier ratios of 1:1 and 1:2 (w/w) were employed for surface modification of MWCNTs. MWCNTs were initially dispersed in THF by ultrasonication (Ultrasonic Processor 750W, Sonics & Materials Inc.) for 10 min. The modifier solution in THF was then slowly added to the dispersion of MWCNTs followed by ultrasonication for another 30 min. Subsequently, the resultant dispersion of MWCNTs−modifier molecules in THF was continuously stirred at room temperature to evaporate the solvent and obtain the dry powder of modified MWCNTs. The resultant mixture of MWCNTs−modifier molecules was then vacuum-dried in an oven at 40 °C for 24 h to remove the traces of THF.

4.4. Preparation of MWCNT-Incorporated HCEs. A highly concentrated w/o emulsion system with ϕ = 93.5 wt % was chosen for the current study. The dispersed phase of the emulsion comprises a supersaturated inorganic salt solution, in which water constitutes 55 wt % and the remaining materials are ammonium sulfate and ammonium chloride salts along with some trace additives. The mixture of a PIBSA-derivative emulsifier in the blend of canola oil and Exxol D130 oil constitutes the continuous phase. A detailed description of the emulsion composition can be found elsewhere.[16]

A high-torque Caframo BDC 1850 mixer along with a high-shear Jiffy impeller (Jiffy Mixer LM, 32 mm diameter) was used to prepare the HCE samples. MWCNTs were initially dispersed in the oil blend, and the resulting oil blend−MWCNT dispersion was gradually incorporated into the aqueous salt solution to prepare the nanotube-incorporated HCEs. The concentration of MWCNTs in the oil blend was varied from 0.25 to 2 wt %, which corresponds to 0.016−0.13 wt % of the total emulsion. The aqueous phase composition and the aqueous-to-oil phase ratio were kept unaltered for all HCE samples. The detailed procedure for the preparation of the nanotube-incorporated HCEs could be found elsewhere.[16,64] It is to be noted that HCEs under study are stabilized by a relatively large amount of emulsifier, and the MWCNTs dispersed in the oil blend do not show any surfactant-like behavior. To obtain the emulsions with identical droplet size and polydispersity, emulsions with varying

DOI: 10.1021/acsomega.8b03179
ACS Omega 2019, 4, 6647−6659

MWCNT concentrations were subjected to different mixing times. The targeted average droplet size of 5 μm was reached with 6−15 min of refining, depending on the level of MWCNT loading. The compositions of different emulsion samples along with their sample codes are presented in Table 2.

Table 2. Sample Codes and Their Composition for the MWCNT-Incorporated Emulsions

	concentration of MWCNTs (wt %)		
sample code	in oil phase	in total emulsion	types of MWCNTs used
neat	0	0	
0.25NT	0.25	0.0163	unmodified, 1:1 **TOPy**-modified, 1:2 **TOPy**-modified, 1:1 **TDPy**-modified, 1:2 **TDPy**-modified
0.5NT	0.5	0.0325	
1NT	1	0.065	
2NT	2	0.13	

4.5. Characterization Techniques. *4.5.1. UV−Visible Spectroscopic Analysis.* UV−visible spectroscopic measurements were performed on dispersions of pristine and modified MWCNTs in THF using a Shimadzu Varian Cary 100 Bio UV−vis spectrometer. Around 1 mg of unmodified/modified MWCNTs was ultrasonicated in 20 mL of THF with a bath-type sonicator (PCi Analytics, India, frequency 20 kHz) for 20 min.

4.5.2. Fluorescence Spectroscopy. Fluorescent spectra were obtained using a Varian Cary Eclipse fluorescence spectrometer. Measurements were carried out on the solutions of noncovalent modifier molecules and dispersions of unmodified and modified MWCNTs in THF. The excitation wavelength was set at 426 nm.

4.5.3. Transmission Electron Microscopic (TEM) Analysis. TEM micrographs of the unmodified and modified MWCNTs were captured using a JEOL JEM-2100 F (Japan) field-emission electron microscope. To prepare samples for TEM investigation, around 1 mg of unmodified/modified MWCNTs was ultrasonicated in 20 mL of THF with a bath-type sonicator (PCi Analytics, 20 Hz) for 20 min. After ultrasonication, the supernatant was carefully pipetted, and a drop of the dispersion was placed on the TEM grid and it was dried under vacuum.

4.5.4. Scanning Electron Microscopic (SEM) Analysis. SEM analyses on unmodified and modified MWCNTs were performed using FEG-SEM (JSM-7600F, Japan) at an accelerating voltage of 10 kV. A MWCNT dispersion in THF was drop-cast on a silicon wafer, after which the wafer was vacuum-dried. The wafer surface was gold-sputtered prior to imaging.

4.5.5. Raman Spectroscopic Analysis. Raman spectroscopic investigations of unmodified and modified MWCNTs were carried out on a HR 800 micro-Raman spectrometer (HORIBA Jobin Yvon, France). The Raman spectra were obtained in the scanning range of 1000−3000 cm^{-1} with an incident laser excitation wavelength of 532 nm.

4.5.6. Fourier Transform Infrared Spectroscopic (FTIR) Analysis. Fourier transform infrared spectroscopic (FTIR) analysis of the unmodified and modified MWCNTs was carried out using a Vertex 80 FTIR spectrometer (Bruker, Germany). The FTIR spectra were recorded over the scanning range of 400−4000 cm^{-1} at room temperature.

4.5.7. Laser Scanning Confocal Microscopic Analysis. Laser scanning confocal microscopic analyses were carried out on an Olympus IX 81 confocal laser scanning microscope. Laser scanning confocal micrographs were captured using a thin layer of the emulsion that was retained between glass slides. The sample preparation for the confocal microscopic investigation could be found elsewhere.[64] The droplet size and droplet-size distribution of the emulsion samples were estimated from the confocal micrographs using the ImageJ software.

4.5.8. Cryo-FEG-SEM Analysis. The dispersion state of MWCNTs in HCEs was examined using a Cryo-FEG-SEM facility: JSM-7600F FEG-SEM with a PP3000T cryo-preparation system, Japan. The Cryo-FEG-SEM micrographs were captured from the fractured surfaces under 5 kV acceleration voltage. The sample preparation for the Cryo-FEG-SEM analysis can be found elsewhere.[64]

■ ASSOCIATED CONTENT

Supporting Information

The Supporting Information is available free of charge on the ACS Publications website at DOI: 10.1021/acsomega.8b03179.

Photographs illustrating the sedimentation observation study of dispersions of modified and unmodified MWCNTs in THF (Figure S1); optical micrographs depicting the effect of the noncovalent modification on the average agglomerate size of MWCNTs in the MWCNT−oil blend dispersions (Figure S2); average size of the MWCNT agglomerates in MWCNT/oil blend dispersions for the unmodified, **TOPy**-, and **TDPy**-modified MWCNTs (Figure S3); fluorescence quenching curves for **TOPy** and **TDPy** with increase in the concentrations of MWCNTs (Figure S4); FTIR spectra of unmodified, 1:1 (w/w) **TOPy**-, and 1:1 (w/w) **TDPy**-modified MWCNTs (Figure S5); NMR, FTIR, UV−visible, and fluorescence spectroscopic analyses of **TOPy** and **TDPy** molecules (Figures S6−S11) (PDF)

■ AUTHOR INFORMATION

Corresponding Author

*E-mail: arupranjan@iitb.ac.in. Tel: +91 22 2576 7634. Fax: +91 22 2572 6975.

ORCID

Sharu Bhagavathi Kandy: 0000-0001-9939-8239

Wenlong Cheng: 0000-0002-2346-4970

Kei Saito: 0000-0002-5726-8775

Arup R. Bhattacharyya: 0000-0002-2099-2655

Notes

The authors declare no competing financial interest.

■ ACKNOWLEDGMENTS

The authors are grateful to Orica Australia Pty. Ltd. for financial support. The authors would also like to acknowledge SAIF, CRNTS, the "Cryo-FEG-SEM Central Facility" and the "Confocal Laser Scanning Microscope Central Facility" of IIT Bombay.

■ REFERENCES

(1) Cameron, N. R. High Internal Phase Emulsion Templating as a Route to Well-Defined Porous Polymers. *Polymer* **2005**, *46*, 1439−1449.

(2) Reynolds, P. A.; Mcgillivray, D. J.; Mata, J. P.; Yaron, P. N.; White, J. W. The Stability of High Internal Phase Emulsions at Low

DOI: 10.1021/acsomega.8b03179
ACS Omega 2019, 4, 6647−6659

Surfactant Concentration Studied by Small Angle Neutron Scattering. *J. Colloid Interface Sci.* **2010**, *349*, 544−553.
(3) Masalova, I.; Foudazi, R.; Malkin, A. Y. The Rheology of Highly Concentrated Emulsions Stabilized with Different Surfactants. *Colloids Surf., A* **2011**, *375*, 76−86.
(4) Solans, C.; Esquena, J.; Azemar, N.; Rodríguez, C.; Kunieda, H. Highly Concentrated (Gel) Emulsions: Formation and Properties. In *Emulsions: Structure, Stability and Interactions*; Petsev, D., Ed.; Elsevier Ltd: London, 2004; pp 511−555.
(5) Lissant, K. J. The Geometry of High-Internal-Phase-Ratio Emulsions. *J. Colloid Interface Sci.* **1966**, *22*, 462−468.
(6) Espelt, L.; Clapés, P.; Esquena, J.; Manich, A.; Solans, C. Enzymatic Carbon-Carbon Bond Formation in Water-in-Oil Highly Concentrated Emulsions (Gel Emulsions). *Langmuir* **2003**, *19*, 1337−1346.
(7) Clapés, P.; Espelt, L.; Navarro, M. A.; Solans, C. Highly Concentrated Water-in-Oil Emulsions as Novel Reaction Media for Protease-Catalysed Kinetically Controlled Peptide Synthesis. *J. Chem. Soc., Perkin Trans. 2* **2001**, *2*, 1394−1399.
(8) Solans, C.; Eequena, J.; Azemar, N. Highly Concentrated (Gel) Emulsions, Versatile Reaction Media. *Curr. Opin. Colloid Interface Sci.* **2003**, *8*, 156−163.
(9) Esquena, J.; Sankar, R.; Solans, C. Highly Concentrated W/O Emulsions Prepared by the PIT Method as Templates for Solid Foams. *Langmuir* **2003**, *19*, 2983−2988.
(10) Sonneville-Aubrun, O.; Bergeron, V.; Gulik-Krzywicki, T.; Jönsson, B.; Wennerström, H.; Lindner, P.; Cabane, B. Surfactant Films in Biliquid Foams. *Langmuir* **2000**, *16*, 1566−1579.
(11) Maekawa, H.; Esquena, J.; Bishop, S.; Solans, C.; Chmelka, B. F. Meso/Macroporous Inorganic Oxide Monoliths from Polymer Foams. *Adv. Mater.* **2003**, *15*, 591−596.
(12) Vílchez, A.; Rodríguez-Abreu, C.; Menner, A.; Bismarck, A.; Esquena, J. Antagonistic Effects between Magnetite Nanoparticles and a Hydrophobic Surfactant in Highly Concentrated Pickering Emulsions. *Langmuir* **2014**, *30*, 5064−5074.
(13) Tshilumbu, N. N.; Kharatyan, E.; Masalova, I. Effect of Nanoparticle Hydrophobicity on Stability of Highly Concentrated Emulsions. *J. Dispersion Sci. Technol.* **2014**, *35*, 283−292.
(14) Tshilumbu, N. N.; Masalova, I. Stabilization of Highly Concentrated Emulsions with Oversaturated Dispersed Phase: Effect of Surfactant/Particle Ratio. *Chem. Eng. Res. Des.* **2015**, *102*, 216−233.
(15) Masalova, I.; Kharatyan, E.; Malkin, A. Y. Multi-Walled Carbon Nanotubes as a Cosurfactant for Highly Concentrated Emulsions. *J. Dispersion Sci. Technol.* **2013**, *34*, 1074−1078.
(16) Bhagavathi Kandy, S.; Simon, G. P.; Cheng, W.; Zank, J.; Joshi, K.; Gala, D.; Bhattacharyya, A. R. Effect of Incorporation of Multiwalled Carbon Nanotubes on the Microstructure and Flow Behavior of Highly Concentrated Emulsions. *ACS Omega* **2018**, *3*, 13584−13597.
(17) Hermant, M. C.; Klumperman, B.; Koning, C. E. Conductive Pickering-Poly(High Internal Phase Emulsion) Composite Foams Prepared with Low Loadings of Single-Walled Carbon Nanotubes. *Chem. Commun.* **2009**, *No. 19*, 2738−2740.
(18) Kim, H.; Ahn, K. H.; Lee, S. J. Conductive Poly(High Internal Phase Emulsion) Foams Incorporated with Polydopamine-Coated Carbon Nanotubes. *Polymer* **2017**, *110*, 187−195.
(19) Hermant, M. C.; Verhulst, M.; Kyrylyuk, A. V.; Klumperman, B.; Koning, C. E. The Incorporation of Single-Walled Carbon Nanotubes into Polymerized High Internal Phase Emulsions to Create Conductive Foams with a Low Percolation Threshold. *Compos. Sci. Technol.* **2009**, *69*, 656−662.
(20) Zhang, X.; Du, Z.; Zou, W.; Li, H.; Zhang, C.; Li, S.; Guo, W. A Porous Elastomeric Polyurethane Monolith Synthesized by Concentrated Emulsion Templating and Its Pressure-Sensitive Conductive Property. *RSC Adv.* **2015**, *5*, 65890−65896.
(21) Cohen, N.; Samoocha, D. C.; David, D.; Silverstein, M. S. Carbon Nanotubes in Emulsion-Templated Porous Polymers: Polymer Nanoparticles, Sulfonation, and Conductivity. *J. Polym. Sci., Part A: Polym. Chem.* **2013**, *51*, 4369−4377.
(22) Sgobba, V.; Guldi, D. M. Carbon Nanotubes - Electronic/Electrochemical Properties and Application for Nanoelectronics and Photonics. *Chem. Soc. Rev.* **2009**, *38*, 165−184.
(23) Herranz, M. Á.; Martín, N. Noncovalent Functionalization of Carbon Nanotubes. In *Carbon Nanotubes and Related Structures:Synthesis, Characterization, Functionalization, and Applications*; Guldi, D. M., Martín, N., Eds.; WILEY-VCH Verlag GmbH & Co. KGaA: Weinheim, 2010; pp 103−134.
(24) Hauke, F.; Hirsch, A. Covalent Functionalization of Carbon Nanotubes. In *Carbon Nanotubes and Related Structures: Synthesis, Characterization, Functionalization, and Applications*; Guldi, D. M., Martín, N., Eds.; WILEY-VCH Verlag GmbH & Co. KGaA: Weinheim, 2010; pp 135−198.
(25) Karimian, H.; Moghbeli, M. R. Conducting Polymerized High-Internal-Phase Emulsion/Single-Walled Carbon Nanotube Nanocomposite Foams: Effect of the Aqueous-Phase Surfactant Type on the Morphology and Conductivity. *J. Appl. Polym. Sci.* **2016**, *133*, No. 43883.
(26) Casas-Solvas, J. M.; Howgego, J. D.; Davis, A. P. Synthesis of Substituted Pyrenes by Indirect Methods. *Org. Biomol. Chem.* **2014**, *12*, 212−232.
(27) Zhang, Y.; Yuan, S.; Zhou, W.; Xu, J.; Li, Y. Spectroscopic Evidence and Molecular Simulation Investigation of the π-π Interaction between Pyrene Molecules and Carbon Nanotubes. *J. Nanosci. Nanotechnol.* **2007**, *7*, 1−10.
(28) Fukushima, T.; Aida, T. Ionic Liquids for Soft Functional Materials with Carbon Nanotubes. *Chem. - Eur. J.* **2007**, *13*, 5048−5058.
(29) Srinivasan, S.; Ajayaghosh, A. Interaction of Carbon Nanotubes and Small Molecules. In *Supramolecular Soft Matter: Applications in Materials and Organic Electronics*; Nakanishi, T., Ed.; John Wiley & Sons, Inc.: Hoboken, New Jersey, 2011; pp 381−406.
(30) Artyukhin, A. B.; Bakajin, O.; Stroeve, P.; Noy, A. Layer-by-Layer Electrostatic Self-Assembly of Polyelectrolyte Nanoshells on Individual Carbon Nanotube Templates. *Langmuir* **2004**, *20*, 1442−1448.
(31) Lou, X.; Daussin, R.; Cuenot, S.; Duwez, A.-S.; Detrembleur, C.; Pagnoulle, C.; Baily/ly, C.; Jérôme, R. Synthesis of Pyerene Containing Polymers and Noncovalent Side-Wall Functionlization of Multi-Walled Carbon Nanotubes. *Chem. Mater.* **2004**, *16*, 4005−4011.
(32) Liu, L.; Wang, T.; Li, J.; Guo, Z. X.; Dai, L.; Zhang, D.; Zhu, D. Self-Assembly of Gold Nanoparticles to Carbon Nanotubes Using a Thiol-Terminated Pyrene as Interlinker. *Chem. Phys. Lett.* **2003**, *367*, 747−752.
(33) Britz, D. A.; Khlobystov, A. N. Noncovalent Interactions of Molecules with Single Walled Carbon Nanotubes. *Chem. Soc. Rev.* **2006**, *35*, 637−659.
(34) Nakashima, N.; Tomonari, Y.; Murakami, H. Water-Soluble Single-Walled Carbon Nanotubes via Noncovalent Sidewall-Functionalization with a Pyrene-Carrying Ammonium Ion. *Chem. Lett.* **2002**, 638−639.
(35) Bhattacharya, S.; Samanta, S. K. Soft-Nanocomposites of Nanoparticles and Nanocarbons with Supramolecular and Polymer Gels and Their Applications. *Chem. Rev.* **2016**, *116*, 11967−12028.
(36) Srinivasan, S.; Praveen, V. K.; Philip, R.; Ajayaghosh, A. Bioinspired Superhydrophobic Coatings of Carbon Nanotubes and Linear π Systems Based on the "Bottom-up" Self-Assembly Approach. *Angew. Chem., Int. Ed.* **2008**, *47*, 5750−5754.
(37) Malicka, J. M.; Sandeep, A.; Monti, F.; Bandini, E.; Gazzano, M.; Ranjith, C.; Praveen, V. K.; Ajayaghosh, A.; Armaroli, N. Ultrasound Stimulated Nucleation and Growth of a Dye Assembly into Extended Gel Nanostructures. *Chem. - Eur. J.* **2013**, *19*, 12991−13001.
(38) Lerner, M. B.; Resczenski, J. M.; Amin, A.; Johnson, R. R.; Goldsmith, J. I.; Johnson, A. T. C. Toward Quantifying the

DOI: 10.1021/acsomega.8b03179
ACS Omega 2019, 4, 6647−6659

Electrostatic Transduction Mechanism in Carbon Nanotube Molecular Sensors. *J. Am. Chem. Soc.* **2012**, *134*, 14318−14321.
(39) McQueen, E. W.; Goldsmith, J. I. Electrochemical Analysis of Single-Walled Carbon Nanotubes Functionalized with Pyrene-Pendant Transition Metal Complexes. *J. Am. Chem. Soc.* **2009**, *131*, 17554−17556.
(40) Provencher, F.; Bérubé, N.; Laprade, J.; Simard, G.; Tant, J.; De, V.; Geerts, Y.; Silva, C.; Côté, M.; Provencher, F.; et al. Large Electronic Bandwidth in Solution-Processable Pyrene Crystals: The Role of Close-Packed Crystal Structure. *J. Chem. Phys.* **2012**, *137*, No. 034706.
(41) Hayer, A.; De Halleux, V.; Kohler, A.; El-garoughy, A.; Meijer, E. W.; Tant, J.; Levin, J.; Lehmann, M.; Gierschner, J.; Cornil, J.; et al. Highly Fluorescent Crystalline and Liquid Crystalline Columnar Phases of Pyrene-Based Structures. *J. Phys. Chem. B* **2006**, *110*, 7653−7659.
(42) de Halleux, V.; Mamdouh, W.; De Feyter, S.; De Schryver, F.; Levin, J.; Geerts, Y. H. Emission Properties of a Highly Fluorescent Pyrene Dye in Solution and in the Liquid State. *J. Photochem. Photobiol., A* **2006**, *178*, 251−257.
(43) Poyekar, A. V.; Bhattacharyya, A. R.; Panwar, A. S.; Simon, G. P.; Sutar, D. S. Influence of Noncovalent Modification on Dispersion State of Multiwalled Carbon Nanotubes in Melt-Mixed Immiscible Polymer Blends. *ACS Appl. Mater. Interfaces* **2014**, *6*, 11054−11067.
(44) Banerjee, J.; Panwar, A. S.; Mukhopadhyay, K.; Saxena, A. K.; Bhattacharyya, A. R. Deagglomeration of Multi-Walled Carbon Nanotubes via an Organic Modifier: Structure and Mechanism. *Phys. Chem. Chem. Phys.* **2015**, *17*, 25365−25378.
(45) Chen, R. J.; Zhang, Y.; Wang, D.; Dai, H. Noncovalent Sidewall Functionalization of Carbon Nanotubes for Protein Immobilization. *J. Am. Chem. Soc.* **2001**, *123*, 3838−3839.
(46) Nelson, D. J.; Rhoads, H.; Brammer, C. Characterizing Covalently Sidewall-Functionalized SWNTs. *J. Phys. Chem. C* **2007**, *111*, 17872−17878.
(47) Mirershadi, S.; Mortazavi, S. Z.; Reyhani, a.; Moniri, N.; Novinrooz, aJ. Effective Condition for Purification of Multi-Walled Carbon Nanotubes by Nitric Acid. *Synth. React. Inorg., Met.-Org., Nano-Met. Chem.* **2009**, *39*, 204−208.
(48) Dresselhaus, M. S.; Dresselhaus, G.; Saito, R.; Jorio, A. Raman Spectroscopy of Carbon Nanotubes. *Phys. Rep.* **2005**, *409*, 47−99.
(49) Hussain, S.; Jha, P.; Chouksey, A.; Raman, R.; Islam, S. S.; Islam, T.; Choudhary, P. K. Harsh. Spectroscopic Investigation of Modified Single Wall Carbon Nanotube (SWCNT). *J. Mod. Phys.* **2011**, *02*, 538−543.
(50) Athalin, H.; Lefrant, S. A Correlated Method for Quantifying Mixed and Dispersed Carbon Nanotubes: Analysis of the Raman Band Intensities and Evidence of Wavenumber Shift. *J. Raman Spectrosc.* **2005**, *36*, 400−408.
(51) Khare, R. A.; Bhattacharyya, A. R.; Panwar, A. S.; Bose, S.; Kulkarni, A. R. Dispersion of Multiwall Carbon Nanotubes in Blends of Polypropylene and Acrylonitrile Butadiene Styrene. *Polym. Eng. Sci.* **2011**, *51*, 1891−1905.
(52) Sreekanth, M. S.; Panwar, A. S.; Pötschke, P.; Bhattacharyya, A. R. Influence of Hybrid Nano-Filler on the Crystallization Behaviour and Interfacial Interaction in Polyamide 6 Based Hybrid Nano-Composites. *Phys. Chem. Chem. Phys.* **2015**, *17*, 9410−9419.
(53) Lakowicz, J. R. *Principles of Fluorescence Spectroscopy*, 3rd ed.; Springer, 2006.
(54) Hedderman, T. G.; Keogh, S. M.; Chambers, G.; Byrne, H. J. Solubilization of SWNTs with Organic Dye Molecules. *J. Phys. Chem. B* **2004**, *108*, 18860−18865.
(55) Chen, J.; Liu, H.; Weimer, W. A.; Halls, M. D.; Waldeck, D. H.; Walker, G. C. Noncovalent Engineering of Carbon Nanotube Surfaces by Rigid, Functional Conjugated Polymers. *J. Am. Chem. Soc.* **2002**, *124*, 9034−9035.
(56) Murakami, H.; Nomura, T.; Nakashima, N. Noncovalent Porphyrin-Functionalized Single-Walled Carbon Nanotubes in Solution and the Formation of Porphyrin-Nanotube Nanocomposites. *Chem. Phys. Lett.* **2003**, *378*, 481−485.
(57) Tomonari, Y.; Murakami, H.; Nakashima, N. Solubilization of Single-Walled Carbon Nanotubes by Using Polycyclic Aromatic Ammonium Amphiphiles in Water - Strategy for the Design of High-Performance Solubilizers. *Chem. - Eur. J.* **2006**, *12*, 4027−4034.
(58) Aurisicchio, C.; Marega, R.; Corvaglia, V.; Mohanraj, J.; Delamare, R.; Vlad, D. A.; Kusko, C.; Dutu, C. A.; Minoia, A.; Deshayes, G. G.; et al. CNTs in Optoelectronic Devices: New Structural and Photophysical Insights on Porphyrin-DWCNTs Hybrid Materials. *Adv. Funct. Mater.* **2012**, *22*, 3209−3222.
(59) Guldi, D. M.; Rahman, G. M. A.; Jux, N.; Balbinot, D.; Tagmatarchis, N.; Prato, M. Multiwalled Carbon Nanotubes in Donor-Acceptor Nanohybrids-towards Long-Lived Electron Transfer Products. *Chem. Commun.* **2005**, 2038−2040.
(60) Guldi, D. M.; Rahman, G. M. A.; Jux, N.; Balbinot, D.; Hartnagel, U.; Tagmatarchis, N.; Prato, M. Functional Single-Wall Carbon Nanotube Nanohybrids-Associating SWNTs with Water-Soluble Enzyme Model Systems. *J. Am. Chem. Soc.* **2005**, *127*, 9830−9838.
(61) Zannotti, M.; Giovannetti, R.; D'Amato, C. A.; Rommozzi, E. Spectroscopic Studies of Porphyrin Functionalized Multiwalled Carbon Nanotubes and Their Interaction with TiO2 Nanoparticles Surface. *Spectrochim. Acta, Part A* **2016**, *153*, 22−29.
(62) Lee, H. W.; You, W.; Barman, S.; Hellstrom, S.; Lemieux, M. C.; Oh, J. H.; Liu, S.; Fujiwara, T.; Wang, W. M.; Chen, B.; et al. Lyotropic Liquid-Crystalline Solutions of High-Concentration Dispersions of Single-Walled Carbon Nanotubes with Conjugated Polymers. *Small* **2009**, *5*, 1019−1024.
(63) Kulisic, N.; More, S.; Mateo-Alonso, A. A Tetraalkylated Pyrene Building Block for the Synthesis of Pyrene-Fused Azaacenes with Enhanced Solubility. *Chem. Commun.* **2011**, *47*, 514−516.
(64) Sharu, B. K.; Simon, G. P.; Cheng, W.; Zank, J.; Bhattacharyya, A. R. Development of Microstructure and Evolution of Rheological Characteristics of a Highly Concentrated Emulsion during Emulsification. *Colloids Surf., A* **2017**, *532*, 342−350.

DOI: 10.1021/acsomega.8b03179
ACS Omega 2019, 4, 6647−6659